International Journal of
INTELLIGENT SYSTEMS AND APPLICATIONS IN ENGINEERING
ISSN:2147-6799 www.ijisae.org Original Research Paper

Skin Cancer Identification using Cat Swarm-Intelligent Generative RNN Algorithm

Amita Shukla[1], **Gopal Krishna Shyam**[2], **Ritu Shree**[3], **Rohaila Naaz**[4]

Submitted: 17/04/2023 **Revised**: 18/06/2023 **Accepted**: 25/06/2023

Abstract: Cancer of the skin is one type of cancer that begins in the skin itself. It occurs when the growth of abnormal skin cells becomes unchecked. Sunlight and artificial tanning sources are the leading causes of skin cancer. However, additional elements, including genetics, a compromised immune system, and exposure to specific toxins, can also influence how it develops. This study suggests utilizing the cat swarm-intelligent generative recurrent neural network (CS-IGRNN) method to identify skin cancer. This research can aid in the early detection and successful treatment of skin cancer. We used an overall total of 22,000 clinical image datasets gathered from the Dermquest and DermIS Digital Databases. The Weiner filter (WF) is used in image preprocessing to eliminate the captured raw images. Gabor filter bank (GFB) processing extracts the features from the enhanced image. Using a CS-IGRNN to categorize cancer images has been proposed as a potential remedy. RNN, one of the cat's swarm-intelligent generating algorithms, provides precise information about pictures and achieves incredibly good outcomes in image classification. Accuracy, precision, f1-score, specificity, and sensitivity are utilized to evaluate the efficacy of the proposed method. It compared to other methods, extensive testing shows that ours is the most effective.

Keywords: *Skin cancer, clinical images, Weiner filter (WF), Gabor filter bank (GFB), cat swarm-intelligent generative recurrent neural network (CS-IGRNN)*

1. Introduction

One One of the most prevalent and lethal forms of cancer, skin cancer, has long been regarded as a public health emergency. The rate at which cases of skin cancer are diagnosed in the West is increasing, according to recent studies. Melanoma is high on the list of skin cancers in terms of prevalence, but there are many others. Melanocytes, the cells that make up the skin's surface, are affected. It has many cell types that contribute to the skin's aging process. It can occasionally be found in a variety of dark hues.

Additionally, it is found in the skin and can be rose pink, royal purple, azure, or even colorless. It is more dangerous and lethal because of how rapidly it can spread [1]. Among all cancers, skin cancer has shown one of the greatest 10-year rises in incidence rates. Given that the skin is the largest organ of the body, it seems sense that skin cancer is the most common type of cancer in people. Melanoma and non-melanoma are the two basic categories into which skin cancers can be separated. Melanoma is a rare type of skin cancer that has a high fatality rate. The American Cancer Society reports that although melanoma skin cancer accounts for just 1% of occurrences overall, it has a higher mortality rate. Melanoma can only develop from melanocytes. When normally growing melanocytes expand uncontrollably, a malignant tumor develops. The human body as a whole is extremely vulnerable. It usually appears on areas of skin that get a lot of suns, like the hands, face, neck, lips, etc. Early detection is key for treating melanoma and other skin cancers; otherwise, the disease may spread to other organs, and the patient would die a painful death. Melanoma has various subtypes, including nodular, superficial spreading, acral, and lentiginous. Squamous cell carcinomas, basal cell carcinomas, and sebaceous gland carcinomas are far more prevalent than melanomas. The upper and middle layers of the epidermis are the sites of origin for BCC, SGC, and SCC, respectively. These cancer cells don't seem to move to other body parts very quickly. Comparatively speaking, no melanoma tumors are simpler to cure than melanoma malignancies [2].

Worldwide, there were approximately 1 million instances of non-melanoma skin cancer in 2018, including 288,000 malignant melanoma (MM) cases. An aging population and limited healthcare resources highlight the importance of accurate diagnosis and practical detection in developing

[1]*Assistant Professor, Department of Computer Science and Business Systems (CSBS), Noida Institute of Engineering and Technology, Greater Noida, Uttar Pradesh, India, Email id: amita.shukla@niet.co.in*

[2]*Professor, Department of Computer Science and Engineering, Presidency University, Bangalore, India, Email Id: gopalkirshna.shyam@presidencyuniversity.in*

[3]*Assistant Professor, Department of Computer Science & Application, Vivekananda Global University, Jaipur, India, Email Id: ritu.shree@vgu.ac.in*

[4]*Assistant Professor, College of Computing Science and Information Technology, Teerthanker Mahaveer University, Moradabad, Uttar Pradesh, India, Email id: rohailanaaz2@gmail.com*

a comprehensive skin cancer prevention strategy. There is growing worried about the long-term sustainability of immunotherapies as their impacts on survival and cost add to the load on an already overcrowded healthcare system. Dermatologists and general practitioners struggle with early skin cancer identification, particularly with MM. Dermoscopy is regarded as the gold standard of therapy. However, a dermoscopy image has so many visual cues that it might be difficult to interpret; dermatologists only have a limited ability to diagnose MM with a diagnostic sensitivity of 40% in objective testing. Dermoscopy training appears to be beneficial for general practitioners.

However, the fact that only 51% of lesions are accurately diagnosed begs for more advancement [3]. The human body exhibits cancer kind as a result of human DNA alterations. Since the sun has been a major factor in the development of skin cancer, utilizing various methods to protect the body from sunlight can lower the risk of getting this form of cancer. Doctors do the initial treatment for skin diseases by making certain observations on the skin, and they follow up with dermoscopy-based medical examinations. Dermoscopy is an aid to diagnosis that involves taking photos with the help of computer technologies. Another factor reducing the chance of a correct diagnosis of skin cancer is the examination of patients by non-specialist physicians. Pathological evaluation of tissue removed by some surgical techniques leads to precise skin cancer diagnosis [4]. Getting a melanoma diagnosis as soon as possible is crucial for effective therapy. Approximately 92% of patients with melanoma who are diagnosed at an early stage will survive for five years. The main challenge in melanoma identification is making a visual distinction between malignant and benign skin lesions. Because of this, even for a seasoned doctor, diagnosing melanoma can be a challenging task. It is difficult to tell what kind of lesion someone has just by looking at them. Dermoscopy is just one imaging technique that has become increasingly popular in recent years [5]. Therefore, we suggested the CS-IGRNN for the detection of skin cancer.

The remaining sections of this research are as follows: Part 2 contains the related works; the proposed methodology is introduced in Part 3; the result and discussion of the study are in Part 4; the conclusion is in Part 5.

2. Related Work

The research [6] discussed the classification abilities of a few well-known algorithms to create a useful computer-aided system for diagnosing skin and breast cancer that would assist physicians and patients. The study investigated the effectiveness of CNN and RNN in evaluating skin lesion images [7] using large datasets from the International Skin Imaging Collaboration (ISIC) collection. Analysis [8], a deep learning model was tested for its ability to detect skin cancer. In this study, we propose a hybrid "context-aware (CA)-CNN-RNN" based on images of skin cancer histology. The research [9] constructed a hybrid classifier-based mammography breast detection model. The "firefly updated chicken-based CSO (FC-CSO)" hybrid meta-heuristic algorithm is used in the optimum region growth segmentation, which is used to separate the tumor from the image. They wanted to implement deep learning techniques for automatic melanoma diagnosis from dermoscopic ideas. Image training was carried out using the "fuzzy-based GrabCut-stacked convolutional neural networks (GC-SCNN)" model [10]. The research [11] proposed using the sparrow search algorithm (SpaSA), a meta-heuristic optimizer, to detect, classify, and segment skin cancer on a threshold basis. The most crucial aspect is the VEP delay P100, which stands for a temporal concept and provides the basis for human interpretation. It's a rather basic strategy, but its success depends on a wide variety of variables [12]. The research [13] provided a unique and robust skin cancer detection model using features fusion. They analyzed the cross-validated model using 1000 ISIC images and achieved 98.4% of detection accuracy. Using Expectation Maximization (EM) and asymmetry analysis, the study [14] proposed a melanoma detection system that combines fusion at the decision level with a Hidden Markov Model (HMM). A study [15] examined whether artificial intelligence can close the alleged diagnostic accuracy gap by comparing dermoscopic (DI) and smartphone-captured pictures (SI) performance metrics.

3. Methodology

The examination of one's skin for any indications of abnormal development or changes that may suggest the existence of skin cancer is an important part of the process of detecting skin cancer, which is a form of cancer that affects the skin.

3.1. Dataset

Dermquest and the DermIS Digital Database were the data sources for the present study [16]. The Dermquest database is an online medical atlas for healthcare practitioners who work with dermatologists. The renowned international editorial boards have assessed and given their seal of approval to the photographs in Dermquest. Over 22,000 clinical photos and a large number of dermatologists are included. DermIS Digital Database is a separate database created for medical image processing applications. It's an image atlas covering various skin cancers with differential diagnoses. It is widely believed that DermIS is the largest such service on the web today. Fig. 1 displays several samples of the Dermquest and DermIS benign and malignant skin cancer images.

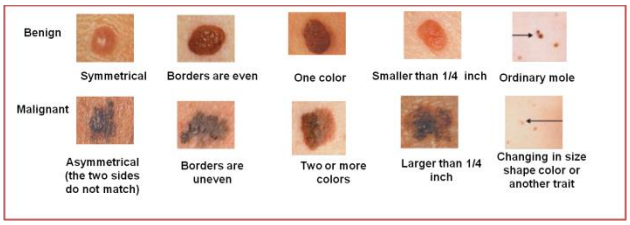

Fig.1. Dermquest and DermIS benign and malignant skin cancer images

3.2. Image preprocessing

Image preprocessing is a subset of data analysis and includes any operations done on raw data before further processing. Weiner filters were used to prepare the basic image for research in the preprocessing.

3.2.1. Weiner filter's

The corrupted images are removed as the computational Weiner filter solution is used. Since converse filtering is used to recover blurred vision, it maintains the ideal balance between converse filtering and signal loss reduction. Assuming that the pictures and disturbance are arbitrary linear processes with known fictitious properties, the filter offers a good approximation. This filter's operation is described as follows:

$$F(g,u) = \frac{J^*(g,u)\eta_T(g,u)}{|D(g,u)|^2\eta_S(g,u)+\eta_F(g,u)} \quad (1)$$

If $\eta_S(g,u)$ and $\eta_E(g,)$ represent the spectral levels of the picture and noise, respectively, whereas D designates the smoothing filter (g,w).

3.3. Gabor filter bank using feature extraction

One such structure intended to mimic neuronal receptive fields is the Gabor filter Bank (GFB). The Gabor frequency bandpass used here is a collection of two-dimensional Gabor filters, each characterized by a unique configuration of its temporal envelope and spectral carrier functions. Where $v_n \, and \, v_f$ are the numbers of semi-cycles under the envelope, n_0 is the carrier frequency, $\omega_n, and \, \omega_f$ are the time and frequency signal processing frequencies, and f_0 is the location of the temporal frame, the Gabor filter can be expressed as a function of the frequency index n and the frame index f. Using a carrier function

$$\gamma(n,f;n_0,f_0,\omega_n,\omega_f,v_n,v_f) = g_{\omega_n}(n-n_0).g_{\omega_f}(f-f_0).z\frac{\pi v_n}{\omega_n}(n-n_0).z\frac{\pi v_f}{\omega_f}(f-f_0) \quad (2)$$

Moreover, the envelope function

$$g_{\omega_c}(c) = \exp(i\omega_c c) \quad (3)$$

Where p is the breadth of the filter

$$z_p(c) = \begin{cases} 0.5 + 0.5\cos\left(\frac{2\pi c}{p}\right), -\frac{p}{2} < c < -\frac{p}{2} \\ 0, otherwise, \end{cases} \quad (4)$$

The filter bank is developed to provide consistent protection in modulation's frequency and time domains. The fundamental frequency in spectral and temporal modulation! Both $\omega_n^j, \ldots, ! \, \omega_n^{X_n}$ and $\omega_f^j, \ldots, ! \, \omega_f^{X_f}$ The number of center frequencies represented by X_n and X_f, respectively, are defined recursively using

$$\omega_n^{j+1} = \omega_n^j \frac{1+\frac{x_n}{2}}{1-\frac{x_n}{2}} \, with \, c_n = t_n = t_n \frac{8}{v_n} \quad (5)$$

$$\omega_f^{j+1} = \omega_f^j \frac{1+\frac{x_f}{2}}{1-\frac{x_f}{2}} with \, x_f = t_f \frac{8}{v_f} \quad (6)$$

The minimum and maximum thresholds are properly linked! $\omega_f^{min}, \omega_f^{max}$, ω_n^{min} and ω_n^{max}. Smaller values for c_n indicate$t_n and \, t_f$ greater filter overlaps. A filter is sensitive to rapid changes in loudness over a large frequency range when ω_n = 0, as opposed to spectral patterns like tonal components when ω_n = 0. In contrast, the output of spectrotemporal filters(ω_f > 0 and $\omega_n \neq 0$) is maximum when the signal exhibits a transient both in time and frequency. There has been research on the most effective GFB settings for wave event classification.

3.4. Cat swarm-intelligent generative RNN algorithm classified for skin cancer detection

In the last step, the cat swarm intelligence generator optimizes the RNN model's optimal parameter settings, leading to increased classification performance. The CSO method is based on two key characteristics of cats, including sleeping and hunting. The cat uses its resting skill to spend time sleeping while staying awake and slowly shifting positions. However, the cat catches the target when it recognizes it. As a result, an arithmetic model with the CSO algorithm's name is created to handle challenging optimization issues. To analyze cat activity, this program defines the tracing and seeking modes. Here is a description of how this mode operates.

Cats spend most of their time resting, yet they are highly perceptive and curious about their environments and the objects inside them. Cats benefit from this behavior because it helps them spot and pursue prey. They sleep excessively about the time they spend actively hunting. CSO was designed by Chu and Tsai (2007), who used cues from this hunting behavior to create a "seeking mode" for when cats are relaxing and a "tracing mode" for when they are following their prey. In CSO, an M-dimensional solution space is populated with cats, each representing a unique solution. This population can be broken down into

two distinct groups. The first set of cats are resting while keeping an eye on their surroundings (this is known as "seeking mode"), while the second set of cats are starting to move and hunt their prey (this is known as "tracing mode"). Using these modes together in the M-dimensional solution space helps CSO get closer to the final answer. Cats need to spend more time in the tracing mode. Hence the number of cats in this subgroup should be modest. This quantity is specified by the relatively insignificant mixture ratio (MR). Once the cats have been separated into these two modes, you'll have access to additional locations and fitness tasks, and the cat with the best answer will be stored in memory. Such operations are iterated repeatedly until the stopping requirements are attained. The steps involved in CSO's computational processes are as follows:

Step 1: To begin, generate the initial population of cats, distribute them uniformly across the M-dimensional solution space (U_m, c) and pick a velocity for each cat randomly between 0 and 1 in the velocity range (U_j, c).

Step 2: Each cat should be given a flag, and depending on the MR value, it should be placed in the searching or tracing mode procedure.

Step 3: Consider each cat's fitness level and save the one with the highest fitness level. The finest answer to date is represented by the location of the best cat (U_{best}).

Step 4: Follow the guidelines for using the cats in seeking or tracing mode as indicated by their respective flags.

Step 5: Terminate the process if the termination criteria in clause (a) are met. Alternatively, perform steps 2 through 5 again.

3.4.1. Seeking Mode (Resting)

The cat is sleeping this way while keeping an eye on its surroundings. The cat chooses its next action when it detects prey or danger. When the cat decides to move, it does it very carefully and gently. When the cat is in the searching mode, it looks into the M-dimensional solution space like it does when it is asleep. The cat knows its location and the several paths it could take to escape the predicament. The self-positioning consideration (SPC), counts of dimension changes (CDC), the searching range of the selected dimension (SRD), and the seeking memory pool (SMP) are the four parameters that the CSO technique uses to express this. The number of copies of each cat found throughout the search process is referred to as SMP. The SRD in the dimension chosen for mutation is the factor that most significantly separates the new and old values. The CDC predicts how many sizes will change. Each of these parameters defines the algorithm's seeking process. The Boolean variable SPC represents the cat's present location as a potential migration location. SPC cannot impact SMP's value.

Below is a description of what happens next in the seeking mode.

Step 1: Make SMP variations of every cat. If the SPC value is true, which results in the creation of SMP-1 copies, the cat's current position is maintained as one of the copies.

Step 2: According to the SRD, create a new location for each copy using (7).

$$U_{dm} = (1 \pm SRD \times Q) \times U_d \quad (7)$$

Where,

U_d=present state;

U_{dm}= position change

Q = a number chosen at random, between 0 and 1.

Step 3: Determine the fitness scores (FS) for new locations. Set the decision chance to 1 if the FS value for each indicated point is precisely 1. If not, use (8) to determine the likelihood of each candidate point being chosen.

Step 4: Choose a new position for cat_j by selecting a random candidate point from the list using the roulette wheel.

$$O_j = \frac{|ET_j - ET_a|}{|ET_{max} - ET_{min}|} \quad (8)$$

Here,

O_j= likelihood of the current contender, cat_j

ET_j= importance of the cat_j condition

ET_{max}= maximal fitness function value

ET_{min}= minimal fitness purpose value

$ET_a = ET_{max}$ for issues with minimizing

$ET_a = ET_{min}$ is used for maximizing issues

3.4.2. Tracing Mode (Movement)

In the tracing mode, a prey-chasing cat is simulated. The cat determines its motion rate and course based on the position and speed of the prey once it has been located while resting (seeking mode). The formula for CSO's cat l velocity in dimension c is:

$$z_{l,c} = z_{l,c} + q_1 \times d_1(U_{best,c} - U_{l,c}) \quad (9)$$

The cat's velocity in dimension d is denoted by z_l; $U_{best,}$ represents c, the optimal cat location; z_c indicates the cat's actual location; d_1 is a constant, and q_1 is a random number between 0 and 1; $z_{l,c}$ represent the cat's exact location. The cat travels around the M-dimensional decision space at this velocity, reporting each new position it assumes. The maximum speed is applied to the cat's rate

if it exceeds the maximum acceleration. Each cat's new role is determined by using.

$$U_{l,c,new} = U_{l,c,old} + z_{l,c} \quad (10)$$

Where,

$U_{l,c,new}$=Cat l new location in dimensions c

$U_{l,c,old}$= Cat l current location in reality$c$.

3.4.5. Termination Criteria

The algorithm is terminated based on the termination criterion. A good termination condition must be chosen for the method to converge correctly. Common CSO termination criteria include running time, iteration count, and degree of improvement.

To determine if an image is healthy, benign, or cancerous, it is run through an optimized RNN. RNNs are a type of NN that uses a sequence of data to generate a direct graph. RNN's output improves when discriminating between recent and historical data because it operates well with time series data. The new LSTM RNN type is capable of handling explosions and gradient masses. The forget, input/output, and memory cell units of an LSTM's three gate gates are its fundamental building components. Using three gate units is an effective method of filtering out noise and isolating what's truly important. GRU is connected to RNN to boost its performance further.

The "forget and output gates" are typically combined by GRU into a single update gateUPc, where the linear interpolation aids in obtaining the current output. Let Tc 1 represent the prior concealed state, and dc Fecomb is the c input feature. Equations (11) and (12) were used to calculate the update gateUPc and reset gateRZcare outputs, respectively.

$$XO_d = B_e(ZF^{cXO}c_d + ZF^{TUP}S_{d-1}) \quad (11)$$

$$QW_d = B_e(ZF^{cQW}c_d + ZF^{TQW}S_{d-1}) \quad (12)$$

Here, we will refer to B_e, which stands for "activation function" or "logistic sigmoid function." The weight function QW_d=$ZF^{cXO}, ZF^{TUP}, ZF^{cQW}, ZF^{TQW}$ needs to be precisely calibrated to close the gap between the measured and real outcomes. In addition to representing the element-by-element multiplication, the candidate state of the remote unit is provided by equation (13).

$$\tilde{S_d} = \tan\left(ZF^{cS} + ZF^{SS}(S_{d-1} \otimes QW_d)\right) \quad (13)$$

Equation (14), which demonstrates how the known activation function S_{d-1} and the candidate state d^{th} are linearly interpolated, gives the GRU hidden activation function S_d.

$$S_d = (1 - XO_d) \otimes \tilde{S_d} + XO_d \otimes S_{d-1} S_d = (1 - XO_d) \otimes \tilde{S_d} + XO_d S_{d-1} \quad (14)$$

Last but not least, the Softmax layer and the entirely linked layer generate three output types: normal, benign, and malignant.

4. Result Analysis

The effectiveness of the suggested model is compared to that of Deep Convolutional Neural Network (DRNN), Support Vector Machine with Random Forest (SVM-RF), Exponential Neighborhood Grey Wolf Optimization (EN-GWO), and Naive Bayes (NB). The proposed model is activated in MATLAB/Simulink. Using the proposed and existing methodologies, performance measures such as accuracy, precision, sensitivity, specificity, and f1-score were analysed.

The dependability of an argument can be calculated by dividing the number of statements by the number of relevant categories. The efficiency of this method depends on the classifier's ability to correctly identify ordinary cases as ordinary and extraordinary events as exceptional. To demonstrate the validity of statistics,

$$Accuracy = \frac{(\text{TP} + \text{TN})}{(\text{TP} + \text{TN} + \text{FP} + \text{FN})} \quad (15)$$

Here,

TP= the proportion of occasions where aberrant images were correctly identified.

FP= is the quantity of falsely discovered abnormal images.

TN= the proportion of times that common images were correctly identified.

FN= is the proportion of images that were incorrectly labeled as usual.

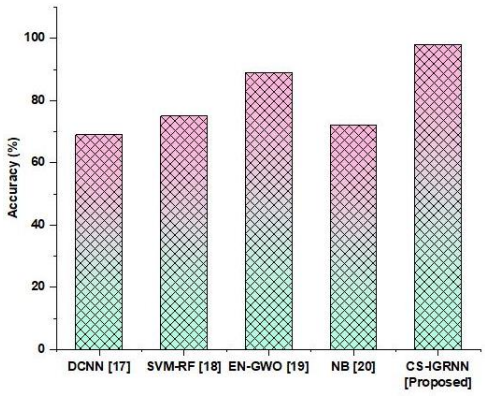

Fig.2. Comparison of the accuracy

Fig. 2 displays the accuracy comparison. It was found that the CS-IGRNN suggested was more accurate than the popular techniques at the time, including DCNN, SVM-RF, EN-GWO, and NB.

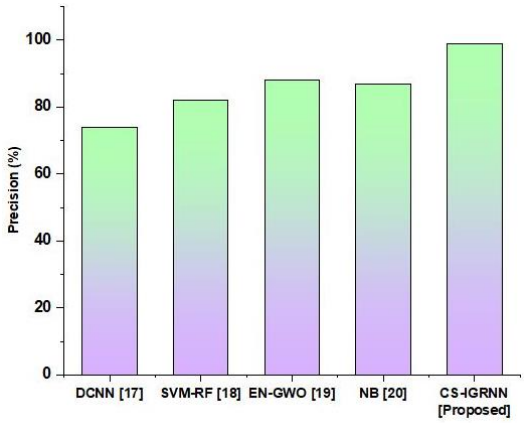

Fig.3. Comparison of the precision

Fig. 3 displays a comparison of the precision. Precision can also be assessed using a positive predictive value (PPV) statistic. Correctly predicting a class from a given sample is one way to evaluate performance. In other words, it contrasts the actual outcomes with the predictions. To determine how precise an observation is, apply the formula below:

$$\text{Precision} = \frac{\text{True positive}}{\text{Total predicted positive}} \quad (16)$$

Compared to other approaches like DCNN, SVM-RF, EN-GWO, and NB, the suggested method CS-IGRNN demonstrates that estimates from a sample image have higher precision.

The sensitivity of a classifier is defined as its ability to detect genuine successes. The degree to which the system can accurately identify instances of skin diseases is directly proportional to the system's sensitivity. The corresponding mathematical expression for this is as follows:

$$\text{Sensitivity} = \frac{TP}{TP+FN} \quad (17)$$

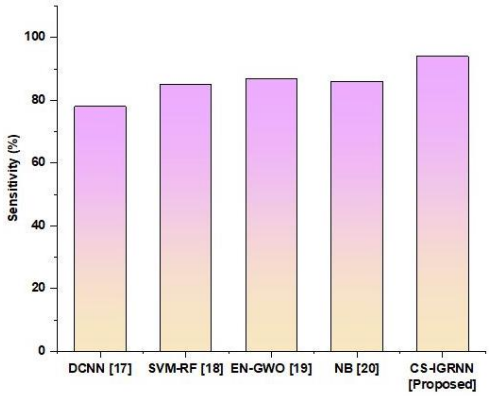

Fig.4. Comparison of the sensitivity

The sensitivity comparison is shown in Fig.4. The suggested CS-IGRNN is more sensitive than previously used methods such as DCNN, SVM-RF, EN-GWO, and NB.

Specificity measures how well a classifier can rule out false positives. The capability of this system to accurately recognize normal circumstances makes it stand out from other similar systems. This can be rephrased using mathematical language as,

$$\text{Specificity} = \frac{TN}{TN+FP} \quad (18)$$

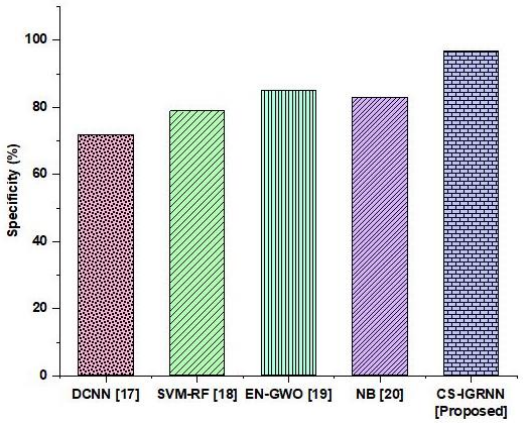

Fig.5. Comparison of the specificity

Fig. 5 is a comparison of the specificity. Existing methods, such as DCNN, SVM-RF, EN-GWO, and NB, do not compare well to the specificity offered by the CS-IGRNN proposal.

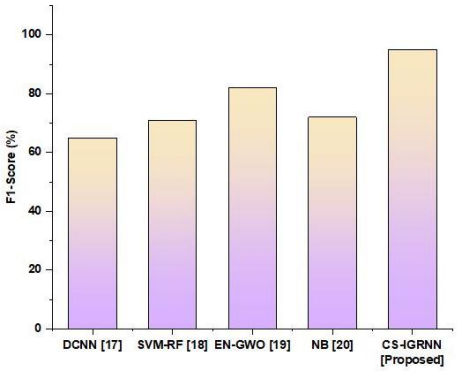

Fig.6. Comparison of the F1-score

Fig.6 displays a comparison of the F1 score. The F1 score takes precision and memory into account as well. The average or median of two distributions is known as the frequency mean. Because of the response time, modern methods for computing averages of numbers can occasionally be more appropriate for ratios than conventional statistical distributions. The suggested approach of CS-IGRNN has a higher F1 score than other methods like DCNN, SVM-RF, EN-GWO, and NB.

5. Conclusion

In the study, we suggested using the CS-IGRNN algorithm for identifying skin cancer. The Dermquest and DermIS Digital Databases provided us with 22,000 clinical picture datasets. The WF eliminates the acquired raw images in image preprocessing. The features are extracted from the

improved image using GFB processing. It has been suggested that a CS-IGRNN may be used to classify cancer images as a possible solution to this problem. This experiment investigated several metrics, including accuracy, precision, sensitivity, and specificity, F1-score. It was suggested to use an AFDR-AM, and its performance was as follows: 98% of accuracy, 99% of precision, 94% of sensitivity, 97 % of specificity, and 95 % of F1 score. The suggested approach outperforms the current systems. The proposed study showed the potential of CS-IGRNN models for identifying, classifying, and segmenting skin cancer, but the recommended method has significant drawbacks. The key disadvantage is instantaneity, with the classifier's training taking up most of the time. High-dimensional features and the slow convergence of the boosting algorithm are the root reasons for this restriction. Obtaining an acceptable precision posed a significant issue, owing to the need for more datasets in this field. Future research aims to improve the performance of the skin cancer segmentation phase using more optimized algorithm approaches and to test the system using more datasets.

References

[1] Ashraf R, Afzal S, Rehman AU, Gul S, Baber J, Bakhtyar M, Mehmood I, Song OY, Maqsood M. Region-of-interest based transfer learning assisted framework for skin cancer detection. IEEE Access. 2020 Aug 6;8:147858-71.

[2] Dildar M, Akram S, Irfan M, Khan HU, Ramzan M, Mahmood AR, Alsaiari SA, Saeed AH, Alraddadi MO, Mahnashi MH. Skin cancer detection: a review using deep learning techniques. International journal of environmental research and public health. 2021 May 20;18(10):5479.

[3] Dascalu A, David EO. Skin cancer detection by deep learning and sound analysis algorithms: A prospective clinical study of an elementary dermoscope. EBioMedicine. 2019 May 1;43:107-13.

[4] Demir A, Yilmaz F, Kose O. Early detection of skin cancer using deep learning architectures: resnet-101 and inception-v3. In2019 medical technologies congress (TIPTEKNO) 2019 Oct 3 (pp. 1-4). IEEE.

[5] Adla D, Reddy GV, Nayak P, Karuna G. Deep learning-based computer aided diagnosis model for skin cancer detection and classification. Distributed and Parallel Databases. 2022 Dec;40(4):717-36.

[6] Swaminathan, Sinan Basarslan M, Kayaalp F. Performance evaluation of classification algorithms on diagnosis of breast cancer and skin disease. InDeep Learning for Cancer Diagnosis 2020 Sep 13 (pp. 27-35). Singapore: Springer Singapore.

[7] Kumar A, Kapelyan A, Vatsa AK. Classification of Skin Phenotype: Melanoma Skin Cancer. In2021 IEEE Integrated STEM Education Conference (ISEC) 2021 Mar 13 (pp. 247-247). IEEE.

[8] Manimurugan S. Hybrid high performance intelligent computing approach of CACNN and RNN for skin cancer image grading. Soft Computing. 2023 Jan;27(1):579-89.

[9] Patil RS, Biradar N. Automated mammogram breast cancer detection using the optimized combination of convolutional and recurrent neural network. Evolutionary intelligence. 2021 Dec;14:1459-74.

[10] Bhimavarapu U, Battineni G. Skin Lesion Analysis for Melanoma Detection Using the Novel Deep Learning Model Fuzzy GC-SCNN. InHealthcare 2022 May 23 (Vol. 10, No. 5, p. 962). MDPI.

[11] Balaha HM, Hassan AE. Skin cancer diagnosis based on deep transfer learning and sparrow search algorithm. Neural Computing and Applications. 2023 Jan;35(1):815-53.

[12] Cheker Z, Chakkor S, Oualkadi AE, Baghouri M, Belfkih R, El Hangouche JA, Laameche J. Performance analysis of VEP signal discrimination using CNN and RNN algorithms. Neuroscience Informatics. 2022 Sep 1;2(3):100087.

[13] Mahum R, Aladhadh S. Skin Lesion Detection Using Hand-Crafted and DL-Based Features Fusion and LSTM. Diagnostics 2022, 12, 2974.

[14] Rastghalam R, Danyali H, Helfroush MS, Celebi ME, Mokhtari M. Skin melanoma detection in microscopic images using HMM-based asymmetric analysis and expectation maximization. IEEE Journal of Biomedical and Health Informatics. 2021 May 18;25(9):3486-97.

[15] Dascalu A, Walker BN, Oron Y, David EO. Non-melanoma skin cancer diagnosis: a comparison between dermoscopic and smartphone images by unified visual and sonification deep learning algorithms. Journal of cancer research and clinical oncology. 2021 Sep 21:1-9.

[16] Zhang N, Cai YX, Wang YY, Tian YT, Wang XL, Badami B. Skin cancer diagnosis based on optimized convolutional neural network. Artificial intelligence in medicine. 2020 Jan 1;102:101756.

[17] Ali MS, Miah MS, Haque J, Rahman MM, Islam MK. An enhanced technique of skin cancer classification using deep convolutional neural network with transfer learning models. Machine Learning with Applications. 2021 Sep 15;5:100036.

[18] Murugan A, Nair SA, Preethi AA, Kumar KS.

Diagnosis of skin cancer using machine learning techniques. Microprocessors and Microsystems. 2021 Mar 1;81:103727.

[19] Mohakud R, Dash R. Skin cancer image segmentation utilizing a novel EN-GWO based hyper-parameter optimized FCEDN. Journal of King Saud University-Computer and Information Sciences. 2022 Nov 1;34(10):9889-904.

[20] Balaji, V.R., Suganthi, S.T., Rajadevi, R., Kumar, V.K., Balaji, B.S. and Pandiyan, S., 2020. Skin disease detection and segmentation using dynamic graph cut algorithm and classification through Naive Bayes classifier. Measurement, 163, p.107922

[21] Mrs. Leena Rathi. (2014). Ancient Vedic Multiplication Based Optimized High Speed Arithmetic Logic . International Journal of New Practices in Management and Engineering, 3(03), 01 - 06. Retrieved from http://ijnpme.org/index.php/IJNPME/article/view/29

[22] Jahan, K. ., Kalyani, P. ., Sai, V. S. ., Prasad, G. ., Inthiyaz, S. ., & Ahammad, S. H. . (2023). Design and Analysis of High Speed Multiply and Accumulation Unit for Digital Signal Processing Applications. International Journal on Recent and Innovation Trends in Computing and Communication, 11(1), 95–102. https://doi.org/10.17762/ijritcc.v11i1.6055